Applied and Computational Mechanics 17 (2023) 105–120

Applied and Computational Mechanics

A fundamental investigation of the interaction and impact of controlled torque ripples on gear mesh dynamics

S. Dave[a,*], J. Neufond[b], R. Nordmann[c], S. Rinderknecht[a]

[a] *Institute for Mechatronic Systems, Technical University of Darmstadt, 64287, Darmstadt, Germany*
[b] *Vibratec SA, 69130, Écully, France*
[c] *Fraunhofer LBF, Bartningstraße 47, 64289, Darmstadt, Germany*

Received 22 May 2023; accepted 26 October 2023

Abstract

Gear trains are plagued by self-excited vibrations that are concentrated at the mesh frequency and its harmonics due to their varying mesh stiffness and deviations from the ideal involute profile. This is even more pronounced in spur gears due to their lower contact ratio in comparison to helical gears. For an electric vehicle, due to the absence of an internal combustion engine, noise and vibration signature of the gearbox becomes an important aspect of the vehicle's comfort. However, the presence of a traction motor offers the advantage of having a potential actuator for actively countering these vibrations without adding any additional weight or packaging constraints. This paper presents a fundamental insight into the effect of introducing controlled torque ripples at the mesh frequency and its harmonics, on the noise and vibration characteristics, and the efficiency of the gear mesh. The study utilises a dynamic model of a single stage gear train that accounts for the time varying mesh stiffness and sliding friction at the gear teeth contact. This model is used to provide an understanding of gear mesh dynamics and their resulting interaction with the imposed torque ripples. The study demonstrates the positive effects that controlled torque ripples can have on the noise and vibration behaviour of gear trains and the underlying mechanics that govern this improvement.

Keywords: gear whine, FxLMS controller, vibration control

1. Introduction

Transmission systems experience vibrations that arise over a wide spectrum of frequencies due to various sources. A significant portion of these are an outcome of the very nature of the gear mesh process. These are self-excited in nature and are concentrated at the gear mesh frequency and its harmonics. They are a consequence of the variation in the mesh stiffness as the teeth move in and out of engagement and deviations from the involute profile of the gear teeth. The vibrations generated at the gear mesh eventually reach the end user in the form of structure borne vibrations and gear whine noise. This can degrade the comfort of vehicles, especially electric vehicles where the lack of a combustion engine makes vibrations more perceptible. Gear whine noise can further restrict efforts to reduce the weight of transmission systems as weight reduction invariably leads to reduced stiffness and degraded noise, vibration and harshness (NVH) response.

Over the years, numerous studies have aimed at improving the NVH behaviour of transmission systems using active solutions, since the periodic nature of gear whine noise makes it particularly suited to such approaches. The approaches vary in terms of control strategies,

*Corresponding author. Tel.: +49 615 116-232 69, e-mail: sidharth.dave@tu-darmstadt.de.
https://doi.org/10.24132/acm.2023.838

actuator types and actuator locations. Some studies target the source of the vibration, i.e., the gear mesh, like the method proposed by Chen and Brennan in [5]. This study used magnetostrictive actuators and accelerometers mounted tangentially on one of the meshing gears and acted directly on the angular acceleration of the gears. Other studies have focused on actively isolating the vibrations from reaching the housing. In [9], Guan presented an active control concept consisting of piezoelectric actuators acting on the vibration transfer path between the gear and the shaft. Here, the actuators not only generate control forces to minimise the vibrations, but also serve as a transmission medium for the mean torque. Other approaches have aimed at countering vibrations by applying a control force on the gear shaft, see [8, 15] and [17]. While these solutions have proven effective in limiting vibrations concentrated at the mesh orders, additional actuators must be integrated.

Electric and hybrid-electric vehicles hold an advantage in this regard as they already have an actuator that can be used to reduce gear whine noise, i.e., the traction motor, making it easier to meet packaging and financial constraints. Such an approach was demonstrated by Benzel and Möckel [3] in which they were able to achieve a net reduction of 12 dB in the housing vibration. In [2], it was further shown that the system is effective for varying speeds and loading conditions, as well. The studies, however, did not elaborate on the interaction between the torque ripples produced by the controller with the gear mesh dynamics.

The filtered-x least mean square (FxLMS) controller is widely used for addressing gear whine noise. However, the choice of actuators and their configurations vary; each offering its advantages and limitations. Using the traction motor can help overcome these limitations. This study presents a fundamental investigation into the interaction between the controlled torque ripples and gear mesh dynamics. This is achieved by means of a lumped mass model of a spur gear train that accounts for the time varying mesh stiffness, sliding friction at the gear contact, and load sharing between the teeth in contact as described in Section 2. The model is then used to simulate a feed-forward FxLMS controller to generate controlled torque ripples, which is described in Section 3. The interaction of the controlled torque ripples with the gear mesh are evaluated and analysed in Section 4.

2. Mathematical model

The study uses a 8 degree of freedom (DOF) model shown in Fig. 1 that is based on the model presented by Song [11] and Brethee [4]. It consists of four torsional DOF that are represented by θ. The other four DOF are translational in nature and are represented by y and x along the line of action (LOA) and in the direction perpendicular to the line of action (PLOA), respectively. The gears are modelled as rigid disks and their mesh stiffness $K_{\mathrm{m}}(t)$ along the LOA is evaluated using a stationary contact analysis described in Section 2.2. The shaft support bearings are modelled as springs (K_{bx} and K_{by}) and dampers (C_{bx} and C_{by}) in two mutually perpendicular directions, i.e., along the PLOA and LOA. The load side, drive side, and shafts are indicated by subscripts 'L', 'd', and 's', respectively. The net normal contact force F_{N} between the two gears acts along the LOA and is a consequence of the applied torque.

2.1. Equations of motion

The terms with subscript 'g' refer to the driving gear with a base radius of r_{bg}, henceforth referred to as 'gear'. The terms with subscript 'p' refer to the driven pinion with a base radius of r_{bp}, henceforth referred to as 'pinion'. Using the Lagrange's equations, the equations of

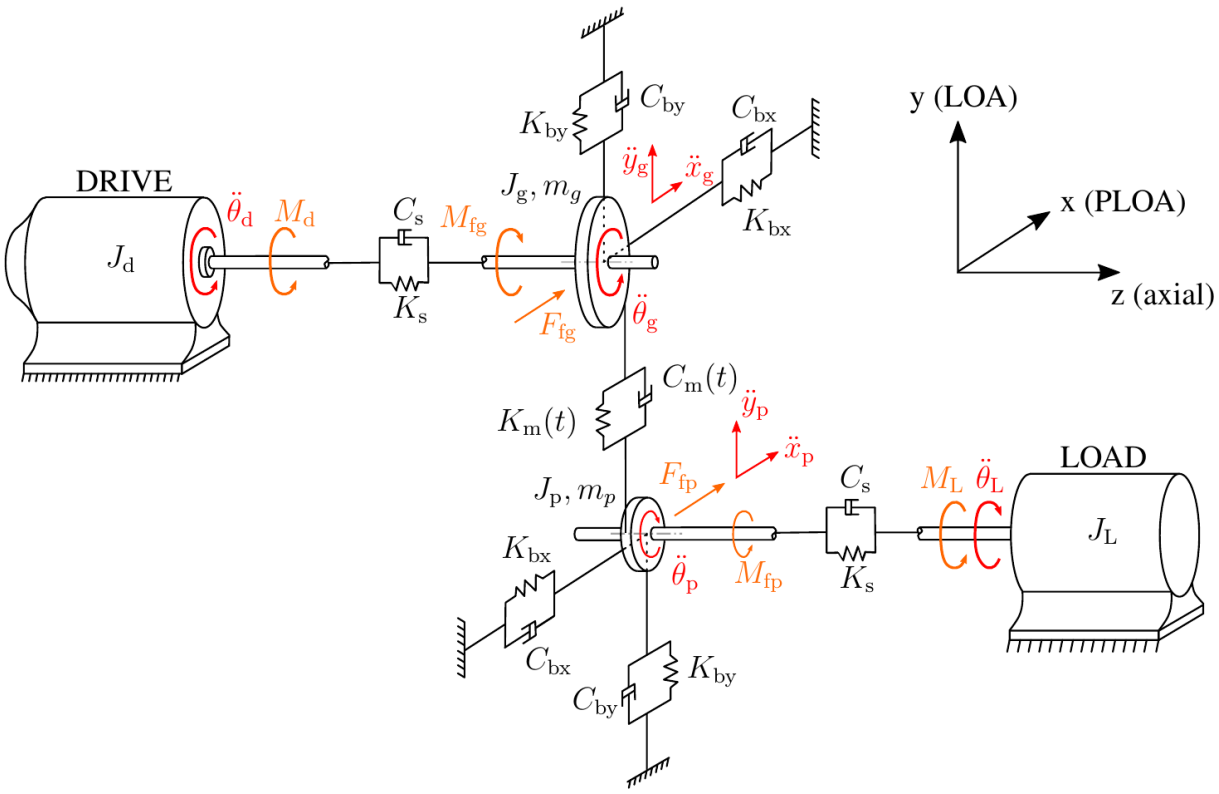

Fig. 1. Model of the system

motion are obtained as

$$J_d\ddot{\theta}_d + C_s(\dot{\theta}_d - \dot{\theta}_g) + K_s(\theta_d - \theta_g) - M_d = 0\,, \tag{1}$$

$$J_g\ddot{\theta}_g + C_s(\dot{\theta}_g - \dot{\theta}_d) + K_s(\theta_g - \theta_d) + r_{bg}F_N + M_{fg} = 0\,, \tag{2}$$

$$J_p\ddot{\theta}_p + C_s(\dot{\theta}_p - \dot{\theta}_L) + K_s(\theta_p - \theta_L) - r_{bp}F_N + M_{fp} = 0\,, \tag{3}$$

$$J_L\ddot{\theta}_L + C_s(\dot{\theta}_L - \dot{\theta}_p) + K_s(\theta_L - \theta_p) + M_L = 0 \tag{4}$$

for the rotational degrees of freedom, and as

$$m_g\ddot{x}_g + C_{bx}\dot{x}_g + K_{bx}x_g - F_{fg} = 0\,, \tag{5}$$

$$m_g\ddot{y}_g + C_{by}\dot{y}_g + K_{by}y_g + F_N = 0\,, \tag{6}$$

$$m_p\ddot{x}_p + C_{bx}\dot{x}_p + K_{bx}x_p - F_{fp} = 0\,, \tag{7}$$

$$m_p\ddot{y}_p + C_{by}\dot{y}_p + K_{by}y_p - F_N = 0 \tag{8}$$

for the translational degrees of freedom. Here, m and J refer to the mass and inertia of the corresponding component, respectively. The forces F_{fp} and F_{fg}, and the moments M_{fp} and M_{fg} are a result of the sliding friction that exists at the point of contact, and are described in Section 2.4. The load M_L is set at a constant value to reach a steady state condition while the drive torque M_d is determined by the controller described in Section 3. The net normal contact force acting between the gear teeth along the LOA is evaluated as

$$\begin{aligned} F_N &= C_m(t)(\dot{\theta}_g r_{bg} - \dot{\theta}_p r_{bp} + \dot{y}_g - \dot{y}_p) + K_m(t)(\theta_g r_{bg} - \theta_p r_{bp} + y_g - y_p) \\ &= C_m(t)\,\dot{\delta} + K_m(t)\,\delta, \end{aligned} \tag{9}$$

where the mesh damping $C_{\mathrm{m}}(\mathrm{t})$ is evaluated using a structural damping factor and the mesh stiffness $K_{\mathrm{m}}(\mathrm{t})$.

The transmission error (TE) is described as the difference between the actual position of the output gear and the position that it would occupy if the gear drive was perfectly conjugate, see [1, 14] and [18]. Under load, this error stems from numerous sources in the geartrain, which include geometry, deflections and deformation, dynamics of the gears, and may further be influenced by assembly errors such as misaligned shafts. This study considers the component of the transmission error that is concentrated at the gear mesh frequency and is a result of the time varying mesh stiffness between the gear teeth in contact. This time varying gear mesh stiffness is an outcome of the periodic variation in the number of teeth in contact and the variation in the stiffness of the gear pair based on the location of the point of contact. At low speeds, in the absence of dynamic effects, this component of the transmission error is referred to as the *static transmission error*. At higher speeds, when the dynamic effects such as the inertia of the rotating components are considered, it is referred to as the *dynamic transmission error*. The terms δ and $\dot{\delta}$ in (9) refer to this component of the transmission error between the two gears in contact and its rate of change along the LOA.

2.2. *Mesh stiffness*

The mesh stiffness of the spur gear pair is evaluated using a stationary contact analysis performed in COMSOL Multiphysics 5.6® by considering a penalty contact between the gear teeth in contact [6]. A soft penalty contact is used to account for the bending and deformation of the gear teeth. The gears are provided with a hinge joint about their centres, which allows rotational motion about the out-of-plane axis. During the simulation, with every iteration, the drive gear and driven pinion are rotated by a fixed incremental value. An additional twist is then imposed on one of the gears and the resulting reaction torque about the hinge joint is recorded. Using the angle of twist and the reaction torque, the torsional stiffness of the gear pair in contact is evaluated at the point of contact. The analysis is performed over a single mesh period and subsequently the mesh stiffness is evaluated along the line of contact. It is then fed into the simulation by means of a look-up table with cubic interpolation using θ_{g} as breakpoints. The mesh stiffness along the LOA is shown in Fig. 2. The driving gear and driven pinion are spur gears with 70 and 48 teeth, respectively. They have a module of 2 mm and a pressure angle of 20° represented by α.

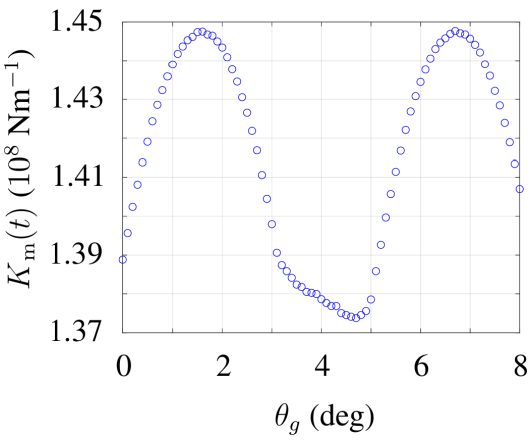

Fig. 2. Mesh stiffness along the LOA

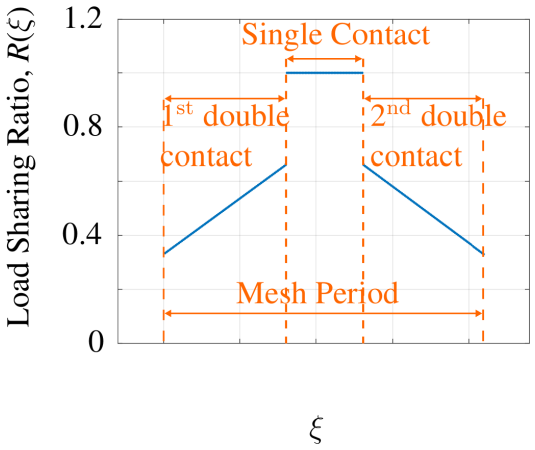

Fig. 3. Load sharing ratio along gear mesh

2.3. Load sharing

The normal contact force in (9) is the equivalent normal contact force acting between the two gears. To determine the sliding friction forces at the contact points, the equivalent normal contact force has to be split into its local contact components. These components are evaluated based on the approach suggested by Pedrero [16]. As a pair of teeth enter the meshing region and establish contact, the load sharing ratio varies from 0.33 to 0.66 during the first phase of double contact, see Fig. 3. It increases to one during single contact and then varies linearly from 0.66 to 0.33 during the second phase of double contact. This behaviour is independent of the gear parameters, such as: the number of teeth, centre distance, profile shift coefficients, etc. At any instant, the normal load between the two pairs of teeth in contact is given by

$$\begin{aligned} F_{\mathrm{N}_2} &= F_{\mathrm{N}}\, R(\xi)\,, \\ F_{\mathrm{N}_1} &= F_{\mathrm{N}}\, [1 - R(\xi)]\,. \end{aligned} \tag{10}$$

Here, the subscripts 1 and 2 refer to the pairs of teeth in contact, see Fig. 4, and $R(\xi)$ refers to the load sharing ratio. Furthermore, ξ is the ratio between the travel length along the LOA and the base circular pitch, and its maximum value is equal to the contact ratio of the gear pair.

2.4. Friction forces and moments

The friction forces act along the PLOA, thus, perpendicular to the normal contact forces. The direction of these friction forces acting on the gear and the pinion, i.e., F_{fg} and F_{fp}, depends on the relative sliding velocity of the teeth in contact. Fig. 4 shows the direction of the friction forces and resulting moments that arise as the contact points move along the LOA, i.e., AE. Point B is where contact is established as the teeth enter the mesh region, while on reaching point D the teeth lose contact. At point C, the point of contact is at the pitch point where the sliding velocity is zero. Points 1 and 2 represent two generic positions before and after the pitch point, respectively, where two pairs of gear teeth are in contact. As a pair of teeth comes

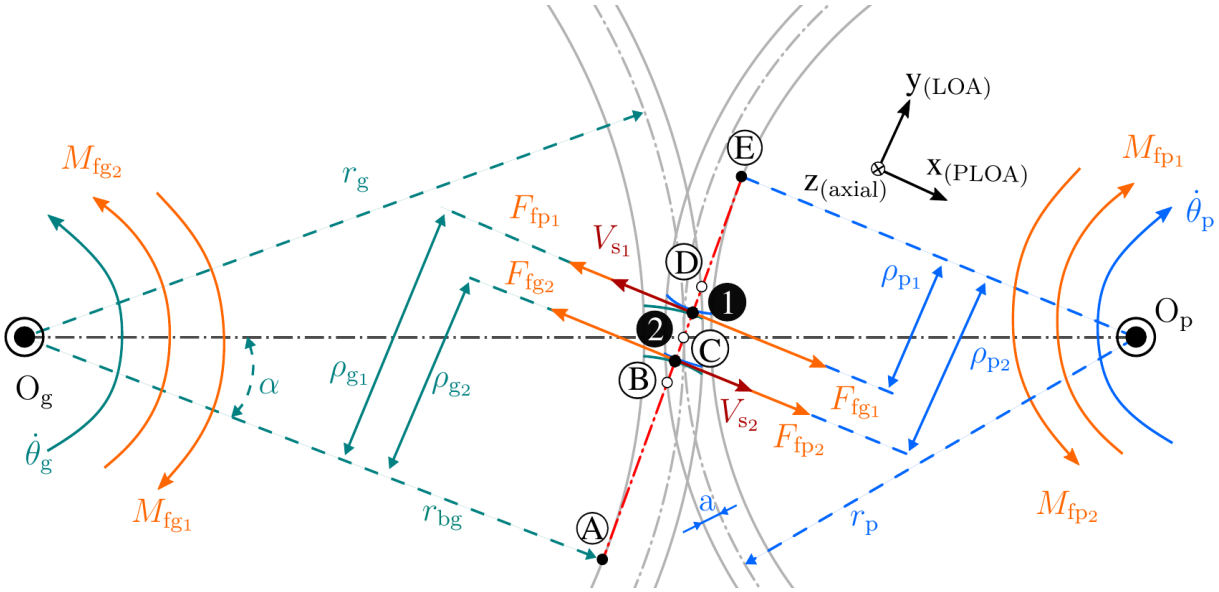

Fig. 4. Forces and moments acting on the driving gear (*left*) and driven pinion (*right*) during the mesh process

in contact at point B, the mesh enters the first double contact phase. As the gears rotate, the previous pair of teeth loses contact on reaching point D and the mesh enters into single contact phase. With further rotation, a new pair of teeth reach point B and establish contact. At this point the mesh cycle enters the second double contact phase which lasts until the pair of teeth lose contact at point D. The mesh process continues to repeat cyclically with the rotation of the gears.

Let i represent the pair of teeth in contact. The friction forces that act at the contact interface, act to minimise the relative sliding velocity between the gear teeth in contact and are given by

$$F_{\mathrm{fg_i}} = \mathrm{sgn}(V_{\mathrm{s_i}})\, F_{\mathrm{N_i}}\, \mu_{\mathrm{i}} = (-1)\, F_{\mathrm{fp_i}}, \tag{11}$$

where $\mathrm{sgn}(.)$ is the signum function, V_{si} represents the sliding velocity, and μ_i represents the coefficient of friction, which is evaluated locally using the elastohydrodynamic lubrication (EHL) approach presented by Xu [19] for the 75W90 lubricant. Using this approach, the local coefficient of friction is evaluated as a function of the slide to roll ratio, i.e., the ratio of the sliding and rolling velocity at the point of contact, which is given as

$$SR_i = \frac{2\,\text{Sliding Velocity}}{\text{Rolling Velocity}} = \frac{2\,V_{\mathrm{s_i}}}{V_{\mathrm{r_i}}}\,. \tag{12}$$

Here, the sliding velocity $V_{\mathrm{s_i}}$ and the rolling velocity $V_{\mathrm{r_i}}$ at the contact points are evaluated as

$$\begin{aligned} V_{\mathrm{s_i}} &= (\dot{\theta}_{\mathrm{g}}\rho_{\mathrm{g_i}} - \dot{x}_{\mathrm{g_i}}) - (\dot{\theta}_{\mathrm{p}}\rho_{\mathrm{p_i}} - \dot{x}_{\mathrm{p_i}}), \qquad i \in [1, \mathrm{ceil}\,(\xi)]\,, \\ V_{\mathrm{r_i}} &= (\dot{\theta}_{\mathrm{g}}\rho_{\mathrm{g_i}} - \dot{x}_{\mathrm{g_i}}) + (\dot{\theta}_{\mathrm{p}}\rho_{\mathrm{p_i}} - \dot{x}_{\mathrm{p_i}}), \qquad i \in [1, \mathrm{ceil}\,(\xi)]\,. \end{aligned} \tag{13}$$

Here, $\mathrm{ceil}(.)$ refers to the operation that rounds up to the smallest integer greater than the input value. Drawing reference to Fig. 4, $\rho_{\mathrm{g_i}}$ and $\rho_{\mathrm{p_i}}$ are the moment arms about which the friction forces generate moments at the gear and pinion centres and these are calculated as

$$\begin{aligned} \rho_{\mathrm{g_i}} &= AB + \mathrm{mod}\left(r_{\mathrm{bg}}\theta_{\mathrm{g}} + (\mathrm{ceil}\,(\xi) - i)\,\sigma,\; 2\sigma\right), \\ \rho_{\mathrm{p_i}} &= AE - \rho_{\mathrm{g_i}}\,. \end{aligned} \tag{14}$$

Here, $\mathrm{mod}(X, Y)$ refers to the modulo operation between X and Y, and is used to evaluate the increase in the length of the moment arm for the gear (ρ_{gi}) as the contact point moves from point B to point D, σ represents the base pitch of the gear pair, and

$$\begin{aligned} AE &= (r_{\mathrm{p}} + r_{\mathrm{g}})\sin\alpha, \\ AB &= (r_{\mathrm{p}} + r_{\mathrm{g}})\sin\alpha - \sqrt{(r_{\mathrm{p}} + a)^2 - (r_{\mathrm{p}}\,\cos\alpha)^2}\,. \end{aligned} \tag{15}$$

Here, a refers to the addendum and, r_{g} and r_{p} refer to the pitch radii of the gear and pinion, respectively.

As a result, the value of the coefficient of friction varies depending on the relative sliding and rolling velocities of the two gear teeth in contact. The value reduces to zero at the pitch point as the sliding velocity reduces to zero and is maximum towards the start and end of the mesh cycle. Additionally, as the point of contact moves across the pitch point, the direction of sliding velocity reverses, causing the friction force to reverse direction, as well. This sudden change in the direction of the friction force acts as an impulse excitation of the gears, leading to lateral vibration along the PLOA ($\ddot{x}_{\mathrm{g}}$ and $\ddot{x}_{\mathrm{p}}$). Furthermore, the friction forces generate moments about

the centres of meshing gears (M_{fg} and M_{fp}), contributing to their angular vibration ($\ddot{\theta}_{\mathrm{g}}$ and $\ddot{\theta}_{\mathrm{p}}$). The amplitude of the forces depends on the local coefficient of friction and the normal contact force, while their direction opposes that of the sliding velocity as shown in (11).

The net friction forces and the corresponding moments are evaluated as the sum of the components at each point of contact

$$F_{\mathrm{fk}} = \sum_{i=1}^{\mathrm{ceil}(\xi)} F_{\mathrm{fk_i}}\,, \qquad M_{\mathrm{fk}} = \sum_{i=1}^{\mathrm{ceil}(\xi)} F_{\mathrm{fk_i}}\,\rho_{\mathrm{k_i}}, \qquad \text{where} \;\; k = p, g. \tag{16}$$

3. Controller

The controlled torque ripples are generated using a FxLMS controller, which has been widely used and discussed in literature to control whine noise in transmission systems. This section provides a brief description of the FxLMS controller that has been implemented based on the work by Kuo [13]. The control signal is generated to minimise the error signal or the residual signal. Making reference to Fig. 5, the error signal can be described by

$$e(t) = d(t) + s(t) * y(t) = d(t) + y'(t)\,. \tag{17}$$

Here, $d(t)$ is the noise, $s(t)$ is the impulse response of the secondary path and $y(t)$ is the output of the actuator through which the control effort is executed. The symbol '$*$' represents convolution. The control output of the actuator takes the form

$$\begin{aligned} y(t) &= w_{\mathrm{c}}\,\cos\phi + w_{\mathrm{s}}\,\sin\phi \\ &= \{w_{\mathrm{c}}\;w_{\mathrm{s}}\}\begin{Bmatrix}\cos\phi\\ \sin\phi\end{Bmatrix} = \underline{w}^T(t)\,\underline{x}(t). \end{aligned} \tag{18}$$

Here, ϕ refers to the phase angle, which is taken as θ_g for this implementation. The signal $\underline{x}(t)$ is the reference signal. The coefficients of the sine and cosine contributions to the actuator

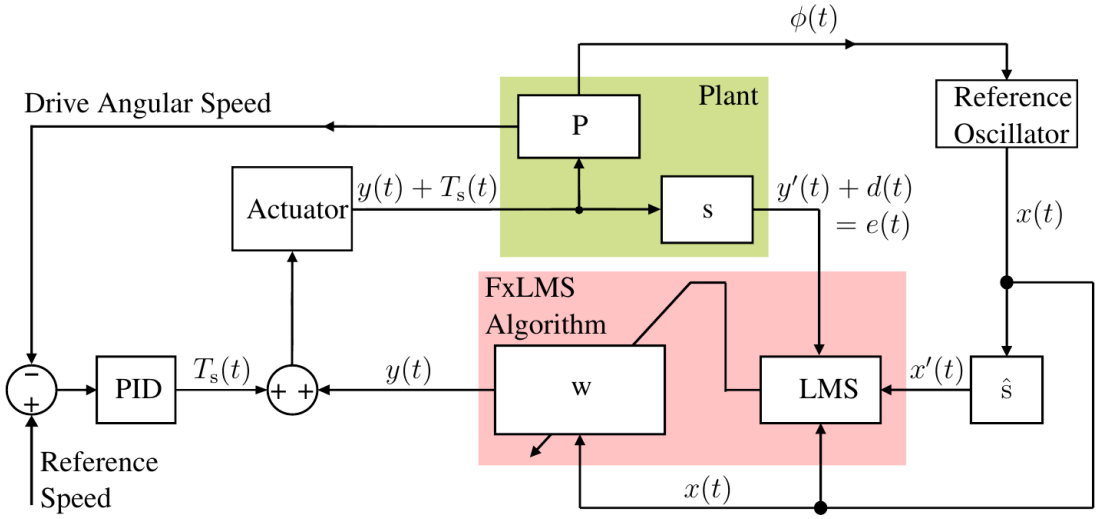

Fig. 5. Structure of the speed (PID) and vibration (FxLMS) controller

output are determined by means of the steepest gradient descent algorithm that minimises the instantaneous squared error. The cost function is, thus, given by

$$\zeta(t) = e^2(t). \tag{19}$$

The coefficients described in (18) are calculated iteratively with every time step (i.e., n) with a step size of κ, i.e., learning rate. The update equation is given by

$$\underline{w}\,[n+1] = \underline{w}\,[n] - \frac{\kappa}{2}\Delta t\,\nabla\zeta\,[n] = \underline{w}\,[n] - \kappa\Delta t\,\begin{Bmatrix}\hat{s}\,[n] * \cos\phi\;\; e\,[n]\\ \hat{s}\,[n] * \sin\phi\;\; e\,[n]\end{Bmatrix}. \tag{20}$$

Here, Δt refers to the size of the time step. The signal $\underline{x}(t)$ is filtered through the estimate of the impulse response of the secondary path $\hat{s}$, to compensate for the phase lag that occurs in the system.

The secondary path of the system is identified by using a chirp signal across the desired frequency range. It is included in the algorithm in the form of a look-up table containing the real and imaginary parts of the secondary path for discrete frequency values, see [12]. For intermediate frequency values, a linear interpolation is performed. This approach offers a computational advantage by replacing convolution with complex multiplication. In addition to the FxLMS controller, the control system uses a proportional-integral-derivative (PID) controller to set the steady state torque T_s that is required to maintain the steady state condition of the system. The controlled torque ripples generated by the FxLMS controller are then superimposed on this steady state torque.

The net output of the controller is the drive torque M_d and is applied on the input shaft by the traction motor, which is assumed to be ideal and given as

$$M_\mathrm{d}(t) = T_\mathrm{s}(t) + y(t)\,. \tag{21}$$

4. Results and discussion

Using the model described above, simulations are performed using Matlab Simulink® with a time step of 10^{-6} s. The simulations are performed for a mesh frequency of 200 Hz and a load of 20 N m. Three controllers named A, B, and C have been implemented, which use $\ddot{\theta}_\mathrm{g}$, $\ddot{y}_\mathrm{g}$, and $\ddot{\theta}_\mathrm{p}$ as the error signals, respectively. They target the first three harmonics of the mesh frequency. The respective error signal and angular velocity of the drive shaft are given as input to the controller and the calculated torque is applied as the drive torque M_d. The simulations are used to compare the behaviour of the system without the controller, i.e., baseline system, and the behaviour of the system when the controller is used, i.e., controlled system.

Fig. 7 shows the impact of Controller A. The torque ripples introduced by the controller cancel out the angular vibration of the driving gear at the first three harmonics of the mesh frequency, Fig. 7a. Furthermore, the controller is also able to reduce the peak-to-peak TE of the gear train, see Fig. 7e. However, despite the reduction in the peak-to-peak TE, the lateral vibrations of the shafts along the LOA only experience minor attenuation, as it is evident from Figs. 7c and 7d. This can be attributed to the fact that although the controller cancels out the angular vibration of the gear, its effect on the angular vibration of the pinion is very low, see Fig. 7b. As a result, the controller is not very effective in dampening the fluctuation in the normal contact forces, which are the source of excitation of $\ddot{y}_\mathrm{g}$ and $\ddot{y}_\mathrm{p}$, see Fig. 6. Thus, the vibration of the shaft and consequently the vibration transfer to the transmission housing experience low attenuation. Hence, the impact on the gear whine noise will be minimal.

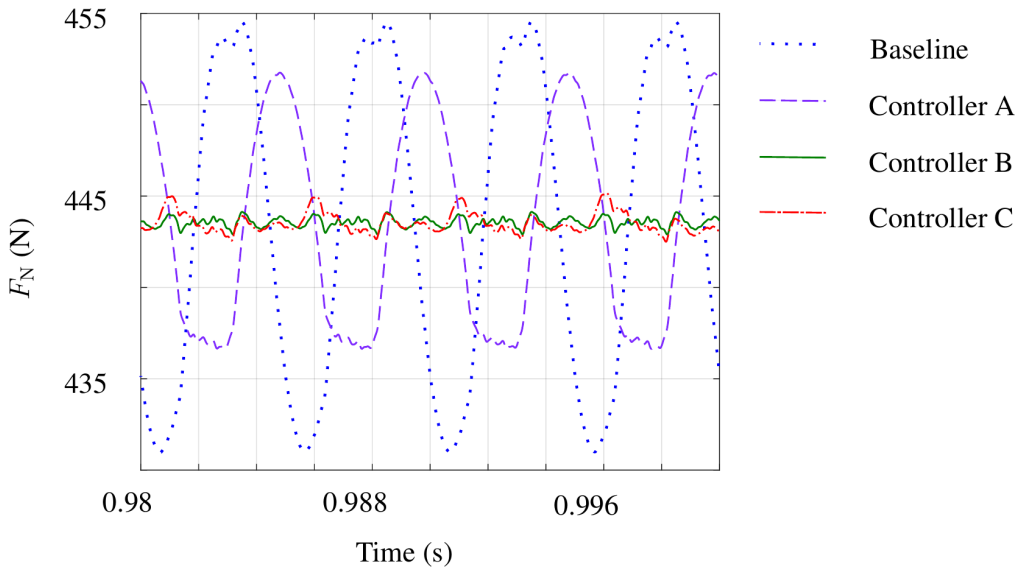

Fig. 6. Normal contact forces

Fig. 7f shows the torque profile determined by the controller. The controller tries to follow the time varying mesh stiffness. This is because by following the mesh stiffness, the controller is able to reduce the peak-to-peak TE and the gear angular vibration, i.e., the error signal for the controller.

As discussed by Guangjian [10] and Rincon [7], the mesh stiffness and TE are related in the following manner:

$$K_{\mathrm{m}}(t) \propto \frac{F_{\mathrm{N}}(t)}{\delta(t)} \quad \Longrightarrow \quad \delta(t) \propto \frac{F_{\mathrm{N}}(t)}{K_{\mathrm{m}}(t)} \quad \Longrightarrow \quad \delta(t) \propto \frac{M_{\mathrm{d}}(t)}{K_{\mathrm{m}}(t)}\,. \tag{22}$$

Here, $\delta(t)$ refers to TE. Thus, if the normal force $F_{\mathrm{N}}(t)$ or the torque $M_{\mathrm{d}}(t)$ follow the same trend as the mesh stiffness, the peak-to-peak TE would decrease, which is also observed in the simulation result. The mean value of the torque determined by the PID controller acting against the mean value of the mesh stiffness establishes the steady state condition while the torque ripples determined by the FxLMS algorithm compensate for the variation in the mesh stiffness.

Fig. 8 shows the results of the simulation with Controller B. The vibrations in the drive shaft along the LOA are a direct result of excitation due to the normal contact forces. Reducing the fluctuation of the normal contact forces about the average normal contact force would result in a reduction of the error signal that is considered here. In Fig. 8c, the effect of the controller on the error signal can be seen. The vibrations of the drive shaft along the LOA are eliminated in the first three orders. Furthermore, since the vibrations of the driven shaft along the LOA are due to the same excitation source, they are also eliminated at the targeted frequencies, see Fig. 8d. The controlled torque ripples introduced by the controller are very effective in dampening the fluctuations in the normal contact force as can be seen in Fig. 6. So even though the reduction in the peak-to-peak TE with Controller B is not as significant as it was with Controller A, Figs. 8e and 7e, respectively, the decrease in the vibration of the shafts along the LOA direction is higher. A reduction in the vibration of the shaft would mean lower transmission of vibration to the gearbox housing and a decrease in gear whine noise.

The angular vibration of the pinion also experiences attenuation at the first three mesh orders (see Fig. 8b) when the acceleration of the drive shaft along the LOA is targeted by Controller B.

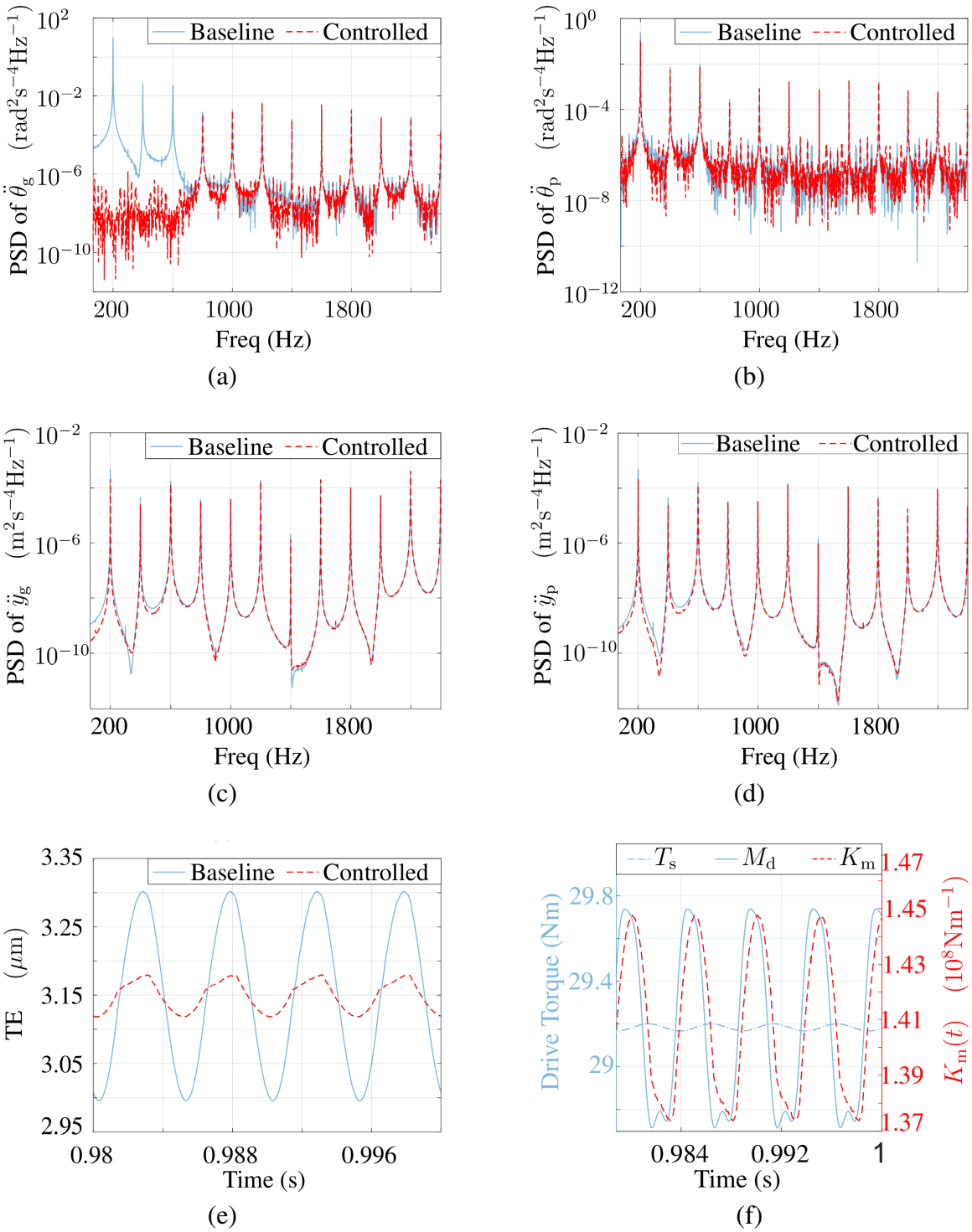

Fig. 7. Results with Controller A: (a) Power spectral density (PSD) of gear angular acceleration, (b) PSD of pinion angular acceleration, (c) PSD of drive shaft acceleration along LOA, (d) PSD of driven shaft acceleration along LOA, (e) transmission error (TE), and (f) torque profile applied by the controller and the gear mesh stiffness

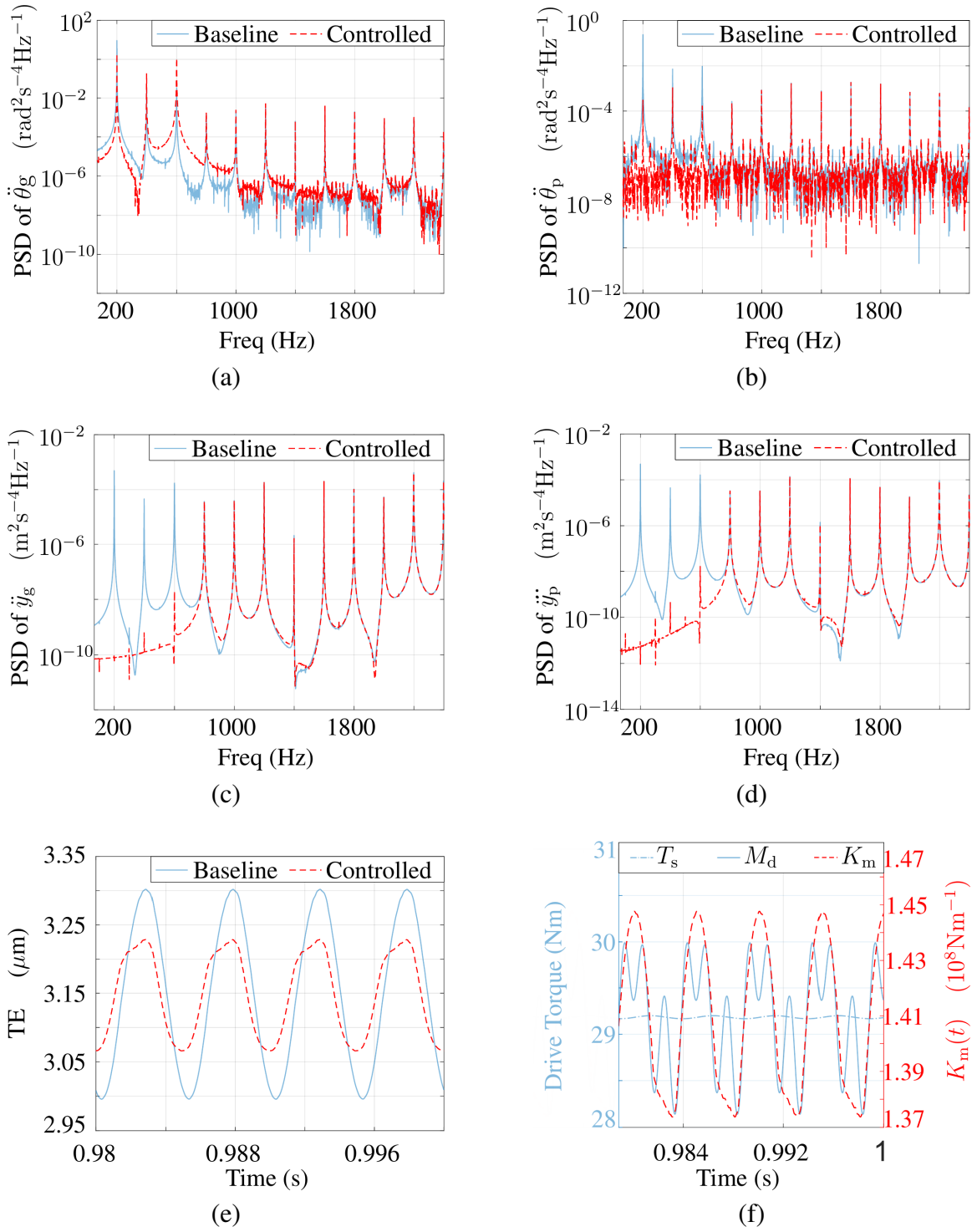

Fig. 8. Results with Controller B: (a) Power spectral density (PSD) of gear angular acceleration, (b) PSD of pinion angular acceleration, (c) PSD of drive shaft acceleration along LOA, (d) PSD of driven shaft acceleration along LOA, (e) transmission error (TE), and (f) torque profile applied by the controller and the gear mesh stiffness

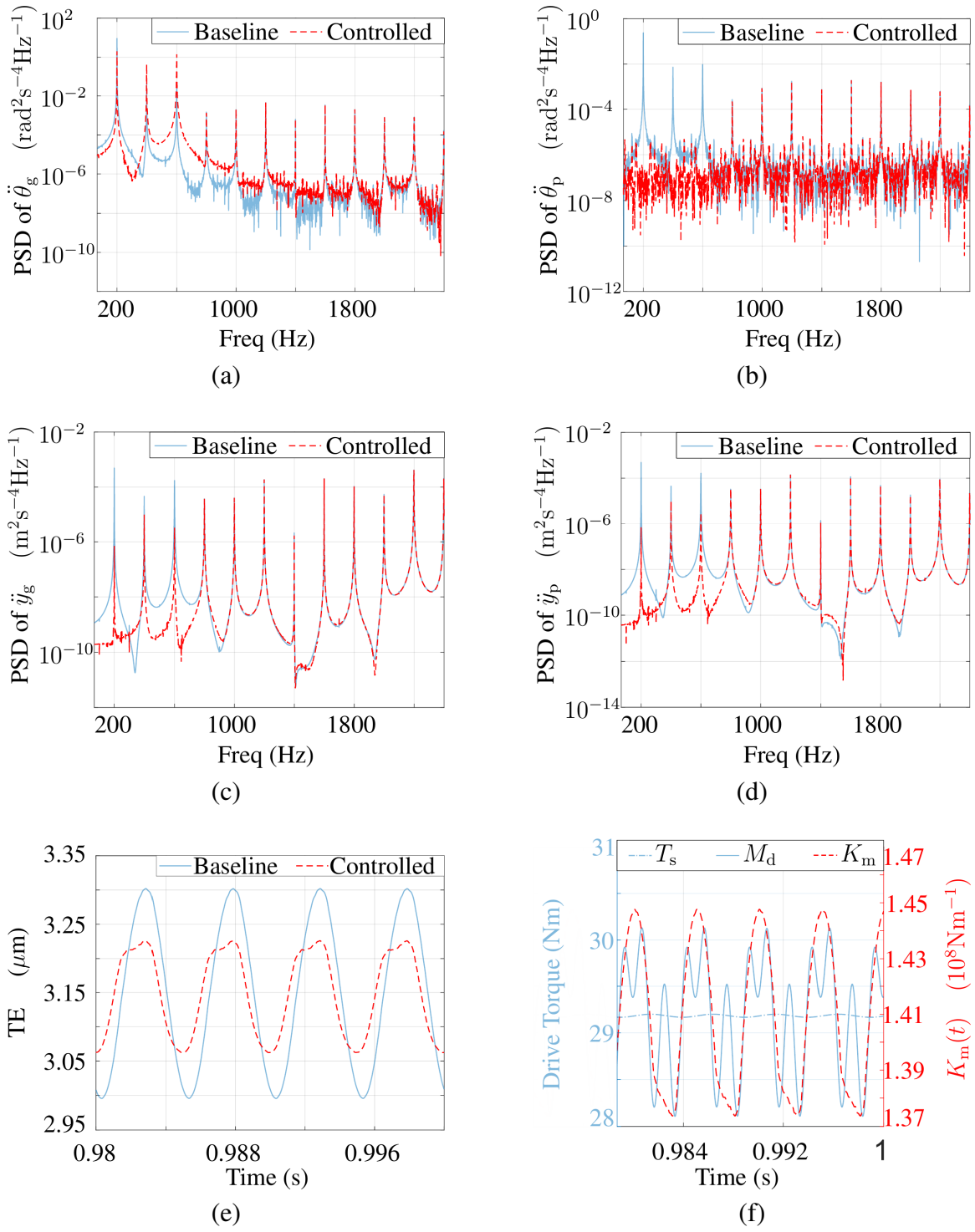

Fig. 9. Results with Controller C: (a) Power spectral density (PSD) of gear angular acceleration, (b) PSD of pinion angular acceleration, (c) PSD of drive shaft acceleration along LOA, (d) PSD of driven shaft acceleration along LOA, (e) transmission error (TE), and (f) torque profile applied by the controller and the gear mesh stiffness

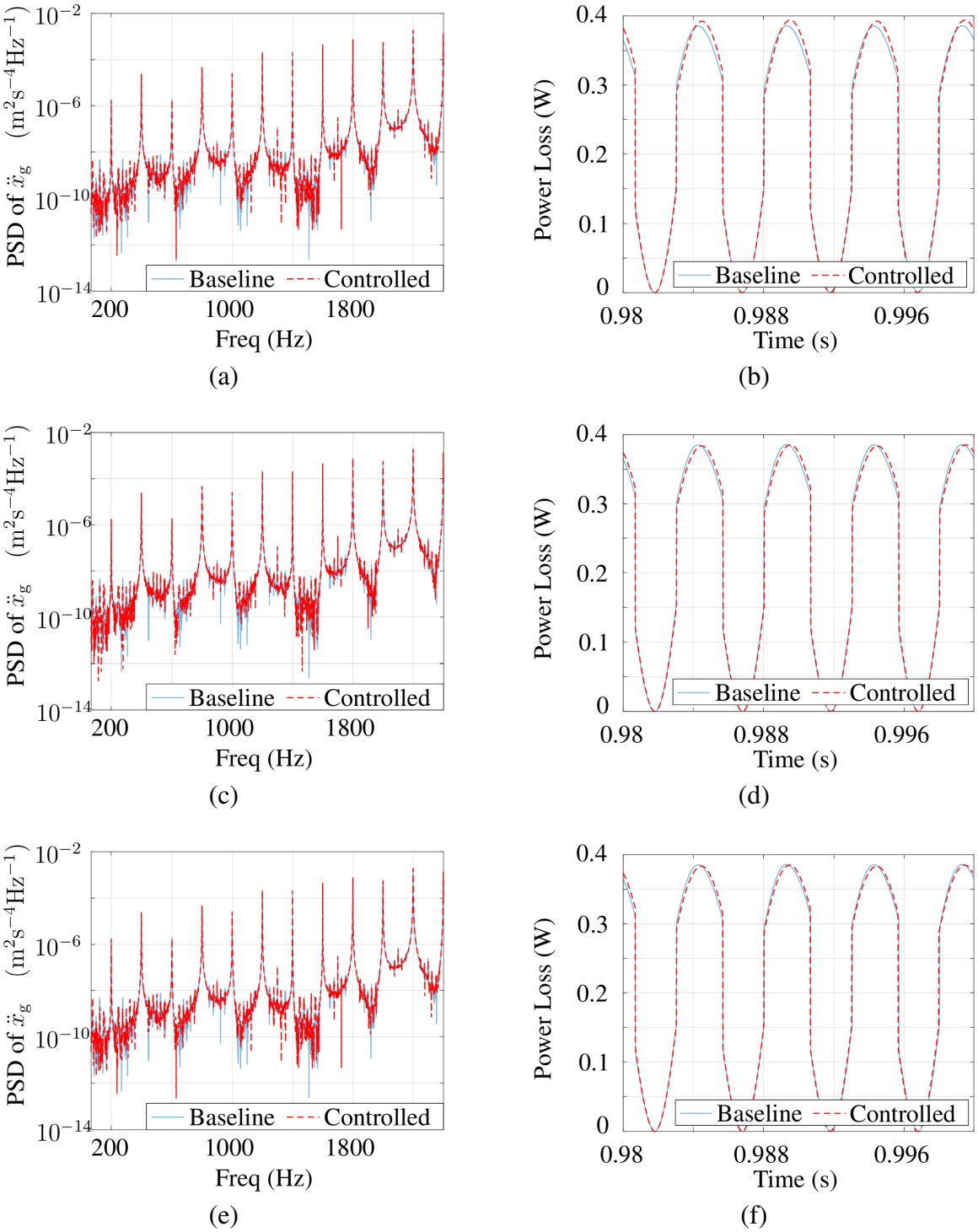

Fig. 10. Response of system to sliding friction: (a) Controller A: PSD of driveshaft acceleration along PLOA, (b) Controller A: Power Loss, (c) Controller B: PSD of driveshaft acceleration along PLOA, (d) Controller B: Power Loss, (e) Controller C: PSD of driveshaft acceleration along PLOA, and (f) Controller C: Power Loss

Considering this, Controller C using the angular vibration of the pinion was set up and the results are shown in Fig. 9. The controller is able to reduce the fluctuations in the normal contact force, Fig. 6. Thus, Controller C is more effective than Controller A in reducing $\ddot{y}_{\mathrm{g}}$ and $\ddot{y}_{\mathrm{p}}$, Figs. 9c and 9d, and Figs. 7c and 7d. Furthermore, the torque profile set up by Controller C is similar to the one that was set up by Controller B, indicating that they have a similar effect.

The vibrations along the PLOA are a direct outcome of the forces due to sliding friction. None of the implemented controllers lead to an improvement in shaft vibration along PLOA, i.e., $\ddot{x}_{\mathrm{p}}$ or $\ddot{x}_{\mathrm{g}}$, as can be seen in Figs. 10a, 10c, and 10e. This indicates that the controllers have minimal impact on the friction forces, which is why the power loss due to sliding friction also remains largely unaffected as can be seen in Figs. 10b, 10d, and 10f.

5. Conclusion and future scope

It has been demonstrated that using controlled torque ripples is an effective approach to reduce the vibrations of a gear train at the mesh orders. However, it is important to select the correct error signal for attenuation. As far as reducing gear whine noise is concerned, limiting the transfer of vibrations to the gearbox housing is crucial. Controlling the angular vibration of the driving gear is not very effective in this regard. Due to the excitation that arises as a result of the time varying mesh stiffness, reducing the angular vibration of the driving gear using Controller A does not result in a comparable decrease in the angular vibration of the driven pinion or the LOA vibrations in the shaft. On the other hand, the opposite approach of using Controller C to attenuate the angular vibrations in the driven pinion proves to be much more effective in attenuating the vibrations along LOA in the shafts. The net effect of controlling the angular acceleration of the driven pinion is similar to directly controlling the vibration of the drive shaft along the LOA.

Controller B is the most effective from the point of view of reducing gear whine noise. This is because vibration in both the shafts are eliminated at the targeted frequencies along the LOA. This would result in a reduction of the vibrations being transferred to the housing and a corresponding reduction in gear whine noise.

The simulations were performed considering an ideal case in order to understand the behaviour of the controllers. In a practical application, the system will be less effective due to the dynamics of the motor, errors in identification of the secondary path, noise from the sensors, and limited resolution of the encoders. While the effect of the controlled torque ripples on the efficiency of the gear train is not very significant in terms of sliding friction losses, generating torque ripples at high frequencies will be challenging for the traction motor and would lead to increased switching losses in the inverter due to the requirement of higher switching frequencies. Furthermore, since the controller uses the angular position of the driving gear to generate controlled torque ripples, its performance will depend on the accuracy and resolution of the signal. Using a high resolution encoder for this purpose can increase the cost of the system and using virtual sensing approaches can be a potential alternative.

Acknowledgement

This study has been performed as part of the LIVE-I project which has received funding from the European Union's Horizon 2020 research and innovation program under Marie Curie grant agreement No 860243.

References

[1] Åkerblom, M., Gear noise and vibration: A literature survey, Trita-MMK 11 (2001) 1–25.

[2] Benzel, T., Möckel, A., Active gear pair vibration control during non-static load and speed with an electronically commutated motor as actuator, Proceedings of the IKMT 2015; 10. ETG/GMM–Symposium Innovative Small Drives and Micro-Motor Systems, Cologne, 2015, pp. 1–6.

[3] Benzel, T., Möckel, A., Multi-channel active gear pair vibration control with an electronically commutated motor as actuator, Proceedings of the 2014 IEEE International Electric Vehicle Conference (IEVC), Florence, 2014, pp. 1–8. https://doi.org/10.1109/IEVC.2014.7056082

[4] Brethee, K. F., Gu, F., Ball, A. D., Frictional effects on the dynamic responses of gear systems and the diagnostics of tooth breakages, Systems Science & Control Engineering 4 (1) (2016) 270–284. https://doi.org/10.1080/21642583.2016.1241728

[5] Chen, M. H., Brennan, M. J., Active control of gear vibration using specially configured sensors and actuators, Smart Materials and Structures 9 (3) (2000) 342–350. https://doi.org/10.1088/0964-1726/9/3/315

[6] COMSOL, Vibrations in a compound gear train, https://www.comsol.com/model/vibrations-in-a-compound-gear-train-36291.

[7] Fernandez del Rincon, A., Viadero, F., Iglesias, M., García, P., de-Juan, A., Sancibrian, R., A model for the study of meshing stiffness in spur gear transmissions, Mechanism and Machine Theory 61 (2013) 30–58. https://doi.org/10.1016/j.mechmachtheory.2012.10.008

[8] Guan, Y., Lim, T., Shepard, W., Experimental study on active vibration control of a gearbox system, Journal of Sound and Vibration 282 (3–5) (2005) 713–733. https://doi.org/10.1016/j.jsv.2004.03.043

[9] Guan, Y. H., Li, M., Lim, T. C., Shepard, W., Comparative analysis of actuator concepts for active gear pair vibration control, Journal of Sound and Vibration 269 (1–2) (2004) 273–294. https://doi.org/10.1016/S0022-460X(03)00072-5

[10] Guangjian, W., Lin, C., Li, Y., Shuaidong, Z., Research on the dynamic transmission error of a spur gear pair with eccentricities by finite element method, Mechanism and Machine Theory 109 (2017) 1–13. https://doi.org/10.1016/j.mechmachtheory.2016.11.006

[11] He, S., Gunda, R., Singh, R., Effect of sliding friction on the dynamics of spur gear pair with realistic time-varying stiffness, Journal of Sound and Vibration 301 (3–5) (2007) 927–949. https://doi.org/10.1016/j.jsv.2006.10.043

[12] Kauba, M., Millitzer, J., Mayer, D., Hanselka, H., Multi-channel narrowband filtered-x-least-mean-square algorithm with reduced calculation complexity, Proceedings of the 5th ECCOMAS Thematic Conference on Smart Structures and Materials SMART, 2011, pp. 49–61.

[13] Kuo, S. M., Morgan, D. R., Active noise control: A tutorial review, Proceedings of the IEEE 87 (6) (1999) 943–975. https://doi.org/10.1109/5.763310

[14] Mark, W. D., Analysis of the vibratory excitation of gear systems: Basic theory, The Journal of the Acoustical Society of America 63 (5) (1978) 1409–1430. https://doi.org/10.1121/1.381876

[15] Montague, G. T., Kascak, A. F., Palazzolo, A., Manchala, D., Thomas, E., Feedforward control of gear mesh vibration using piezoelectric actuators, Shock and Vibration 1 (1994) 473–484. https://doi.org/10.1155/1994/959651

[16] Pedrero, J. I., Pleguezuelos, M., Artés, M., Antona, J. A., Load distribution model along the line of contact for involute external gears, Mechanism and Machine Theory 45 (5) (2010) 780–794. https://doi.org/10.1016/j.mechmachtheory.2009.12.009

[17] Rebbechi, B., Howard, C. Q., Hansen, C. H., Active control of gearbox vibration, Proceedings of the Active Control of Sound and Vibration Conference, Fort Lauderdale, 1999, pp. 295–304.

[18] Tharmakulasingam, R., Transmission error in spur gears: Static and dynamic finite-element modeling and design optimization, Ph.D. thesis, Brunel University School of Engineering and Design, 2010.

[19] Xu, H., Development of a generalized mechanical efficiency prediction methodology for gear pairs, Ph.D. thesis, Ohio State University, 2005.